Available online at www.sciencedirect.com
SCIENCE DIRECT®
Journal of Sound and Vibration 267 (2003) 279–299
JOURNAL OF SOUND AND VIBRATION
www.elsevier.com/locate/jsvi

Influence of non-linear forces on beam behaviour in flutter conditions

S. Tizzi*

Aerospace and Astronautics Department, University of Rome "La Sapienza", Via Eudossiana 16, 00184 Rome, Italy

Received 19 October 2001; accepted 8 October 2002

Abstract

Appropriate researches on non-linear panel flutter behaviour have been already performed by many authors. In most cases the intent of them focuses on the limit cycle determination, with particular interest towards its amplitude versus the flow dynamic pressure. This paper deals first with a study of all the solutions without damping of beam flutter versus the vibration frequency in non-linear post-critical conditions. A numerical model, which takes into account the influence of the non-linear contribution of the structural forces, due to the axial stretching of the beam, has been implemented. A complete analysis of all the possible non-linear solutions without damping leads to the possibility of characterizing the most appropriate conditions for the presence of the post-critical panel flutter limit cycles. Then the complete model, which also takes into account aerodynamic damping, has been utilized, according to the "Piston Theory", to verify the state evolution of the fluttering damped beam towards the limit cycle, which is very near to the undamped vibrating beam state with minimum amplitude. This convergence test is an interesting aspect of the numerical results.

1. Introduction

The subject at hand has already been treated by many authors and different numerical algorithms have been set-up for its solution.

Dowell [1,2] applied the Galerkin method [3,4] to integrate over the panel surface and to arrive at a system of non-linear differential equations in time.

*Corresponding authtor. Tel.: +06 44585 325; fax: +06 44585 640.
E-mail address: s.tizzi@caspur.it (S. Tizzi).

0022-460X/03/$ - see front matter
doi:10.1016/S0022-460X(03)00177-9

Kuo et al. [5] likewise applied the Galerkin method to limit the variable dependence on time and utilized trigonometric functions to set-up two systems of equations, whose unknowns are the vibration frequencies and the temporal coefficients of the describing functions.

Smith and Morino [6] were interested in the general theory of the stability analysis of non-linear differential systems and built an algorithm, which was applied to the particular case of non-linear flutter of panels in post-critical conditions.

Also the finite element method (FEM) [7,8] has been utilized for flutter analysis of both isotropic and composite materials [9], using unsteady third order piston theory aerodynamics [10,11].

In this work a numerical procedure [12–14], which arises from the Rayleigh–Ritz method [3,15], has been applied and developed. Since the boundary conditions of the structural problem are homogeneous, both linear and non-linear structural forces are conservative [4,16] and it is possible to form their potential function. The knowledge of this, along with the kinetic energy and aerodynamic forces, allows the application of the Lagrange equations [16] in order to arrive at a system of differential equations in time. There are appropriate algorithms for the step-by-step integration process.

It is possible to find the area, where there exists possibility of a limit cycle, from the behaviour of the modal shape amplitude verses the frequency of the beam flutter without aerodynamic damping, which lies in the neighbourhood of the solution with minimum amplitude.

Two cases of a simply supported and clamped beam, respectively, have been considered. It has been possible to verify the presence of the limit flutter cycle in this area, by utilizing the complete model which takes into account also the aerodynamic damping.

To validate the results of the Ritz procedure, the Galerkin method has been employed in the simply supported beam case, as in Dowell's model [1,2], whereas FEM has been used also in the clamped beam case.

2. Mathematical model

A vibrating beam, simply supported or clamped at both ends, and exposed to a high supersonic flow along the axis x, must be considered, as in Fig. 1.

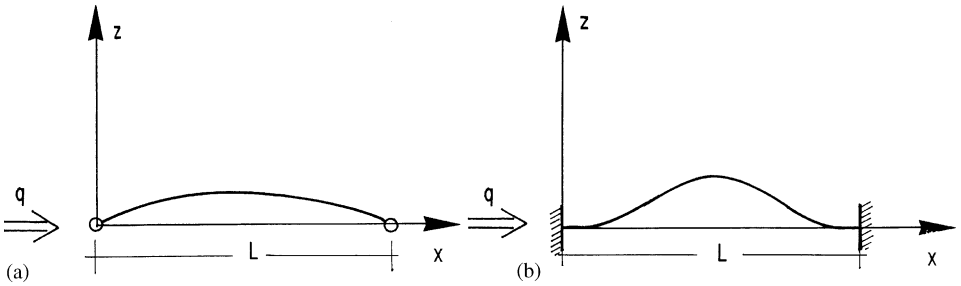

Fig. 1. Beam, simply supported or clamped at both ends, exposed to an high supersonic flow.

The beam flutter constitutive equation, taking into account also the non-linear structural contribution, due to axial stretching, reads [1,17]

$$EI\frac{\partial^4 w}{\partial x^4}+\mu\frac{\partial^2 w}{\partial t^2}-N_x\frac{\partial^2 w}{\partial x^2}+p_z b_w=0, \tag{1}$$

where I is the flexural moment of inertia, E is the modulus of elasticity, μ is the beam mass per unit length, $w(x,t)$ is the flexural displacement, and b_w is the beam width. The geometric boundary conditions must be imposed, for which the flexural displacement vanishes at both ends, but in the case of clamped beam also its first derivative with respect to x vanishes. If the Galerkin method is utilized in the simply supported beam case, also the natural boundary conditions must be imposed, for which also the flexural displacement second derivative with respect to x vanishes at both ends. The resulting axial strength N_x [17] is

$$N_x=EA_s\left[\frac{\partial u}{\partial x}+\frac{1}{2}\left(\frac{\partial w}{\partial x}\right)^2\right], \tag{2}$$

where $u(x,t)$ is the axial displacement, and A_s is the beam cross-sectional area. The aerodynamic pressure p_z according the quasi-steady high supersonic theory [1,10], can be written as

$$p_z=\frac{2q}{\beta}\left[\frac{\partial w}{\partial x}+\frac{(M_{ach}^2-2)}{(M_{ach}^2-1)}\frac{1}{U_\infty}\frac{\partial w}{\partial t}\right], \tag{3}$$

where the notation is defined in Appendix D. This has been obtained by the "Piston Theory" of an high supersonic idealized flow. The first term give rise to coupling between different vibrating modes, whilst the second term is the aerodynamic damping, which is not considered when the undamped vibrating beam solution is requested.

Together with Eq. (1) the axial equilibrium equation has to be considered [17]:

$$\frac{\partial N_x}{\partial x}=EA_s\left[\frac{\partial^2 u}{\partial x^2}+\frac{\partial w}{\partial x}\frac{\partial^2 w}{\partial x^2}\right]=0, \tag{4}$$

because there are not axial distributed forces and the section area A_s is supposed constant. Thus it is true that the axial strain

$$\varepsilon_x(t)=\frac{\partial u}{\partial x}+\frac{1}{2}\left(\frac{\partial w}{\partial x}\right)^2 \tag{5}$$

together with the resulting strength N_x, are constant along the axial beam co-ordinate x, but with the inherent in time non-linearities.

Since ε_x is constant versus x and $u(x,t)=0$ for $x=0$ and L, integration of Eq. (5) leads to

$$\varepsilon_x(t)L=\int_0^L\left[\frac{\partial u}{\partial x}+\frac{1}{2}\left(\frac{\partial w}{\partial x}\right)^2\right]\mathrm{d}x=\frac{1}{2}\int_0^L\left(\frac{\partial w}{\partial x}\right)^2\mathrm{d}x=\frac{1}{2}L\overline{\left(\frac{\partial w}{\partial x}\right)^2}. \tag{6}$$

Consequently, the axial strain is equal to half of the mean square value of the first derivative $\partial w/\partial x$, that is

$$\varepsilon_x(t)=\frac{1}{2}\overline{\left(\frac{\partial w}{\partial x}\right)^2}. \tag{7}$$

Thus, Eq. (1) can be also written as

$$EI\frac{\partial^4 w}{\partial x^4}+\mu\frac{\partial^2 w}{\partial t^2}+\sigma\frac{\partial w}{\partial x}-EA_s\frac{1}{2}\overline{\left(\frac{\partial w}{\partial x}\right)^2}\frac{\partial^2 w}{\partial x^2}+c_d\frac{\partial w}{\partial t}=0, \tag{8a}$$

where

$$\sigma=\frac{2q}{\beta}b_w, \qquad c_d=\frac{2q}{\beta}\frac{b_w}{U_\infty}\frac{(M_{ach}^2-2)}{(M_{ach}^2-1)} \tag{8b}$$

and in non-dimensional form

$$\frac{\partial^4 W}{\partial \xi^4}+\lambda\frac{\partial^2 W}{\partial \tau^2}+\sigma_d\frac{\partial W}{\partial \xi}-\frac{\alpha}{2}\overline{\left(\frac{\partial W}{\partial \xi}\right)^2}\frac{\partial^2 W}{\partial \xi^2}+\gamma\frac{\partial W}{\partial \tau}=0, \tag{9a}$$

where

$$\xi=\frac{x}{L}, \quad W(\xi)=\frac{w}{L}, \quad \lambda=\frac{\mu L^4}{EIT_o^2}, \quad \sigma_d=\frac{\sigma L^3}{EI}, \tag{9b}$$

$$\tau=\frac{t}{T_o}, \quad \alpha=\frac{A_s L^2}{I}, \quad \gamma=\frac{c_d L^4}{EIT_o}, \tag{9c}$$

where T_o is a reference time. A series expansion for $W(\xi)$ in the form

$$W(\xi,\tau)=\sum_{i=1}^{N} W_i(\tau)f_i(\xi) \tag{10}$$

is assumed, where $f_i(\xi)$ are polynomial functions satisfying only the geometric boundary conditions, as in the Ritz method [3,15].

The repeated indices rule will be utilized in the following equations. It is possible to build the potential of the linear structural forces, corresponding to the fourth derivative of W with respect to ξ in Eq. (9a), which can be written as

$$\mathscr{U}_l=\tfrac{1}{2}k_{ij}W_iW_j, \quad i,j=1,2,\ldots,N, \tag{11}$$

where the stiffness matrix elements k_{ij} have been already determined [13]. The kinetic energy can be written as

$$\mathscr{T}=\tfrac{1}{2}m_{ij}\dot{W}_i\dot{W}_j, \quad (\cdot)=\partial()/\partial\tau, \quad i,j=1,2,\ldots,N, \tag{12}$$

where m_{ij} are the mass matrix elements:

$$m_{ij}=\lambda c_{ij} \tag{13}$$

and c_{ij} are the coupling elements between the describing functions:

$$c_{ij}=\int_0^1 f_i(\xi)f_j(\xi)\,\mathrm{d}\xi, \quad i,j=1,2,\ldots,N \tag{14}$$

likewise previously determined [13].

If expression (7) of ε_x and the series expansion (10) are taken into account, one obtains

$$\varepsilon_x(t) = \frac{1}{2}\overline{\left(\frac{\partial W}{\partial \xi}\right)^2} = \frac{1}{2}\varphi_{ij} W_i W_j, \quad i,j = 1,2,\ldots,N, \tag{15a}$$

where

$$\varphi_{ij} = \int_0^1 \frac{\partial f_i(\xi)}{\partial \xi}\frac{\partial f_j(\xi)}{\partial \xi}\,\mathrm{d}\xi \tag{15b}$$

which can be computed as shown in Appendix A.

Since the strain in Eq. (15a) is constant throughout the beam length, the potential of the non-linear structural forces, corresponding to the fourth term in Eq. (9a), can be easily evaluated and written as

$$\begin{aligned}\mathscr{U}_{nl} &= \frac{1}{2}\alpha\int_0^1 \varepsilon_x^2\,\mathrm{d}\xi = \frac{1}{2}\alpha\varepsilon_x^2 \\ &= \frac{\alpha}{8}\left[\overline{\left(\frac{\partial W}{\partial \xi}\right)^2}\right]^2 = \frac{\alpha}{8}\varphi_{ij}\varphi_{kl} W_k W_l W_i W_j, \quad i,j,k,l = 1,2,\ldots,N.\end{aligned} \tag{16}$$

If the Lagrangian $\mathscr{L}$ [16] is introduced:

$$\mathscr{L} = \mathscr{T} - \mathscr{U}_l - \mathscr{U}_{nl}, \tag{17}$$

the generic ith constitutive equation reads

$$\frac{\mathrm{d}(\partial\mathscr{L}/\partial\dot{W}_i)}{\mathrm{d}\tau} - \frac{\partial\mathscr{L}}{\partial W_i} + F_i^{(a)} = 0, \quad i = 1,2,\ldots,N, \tag{18}$$

where $F_i^{(a)}$ are the generalized aerodynamic forces acting on ith degree of freedom, corresponding to the generic coefficient W_i of the flexural displacement W series expansion (10), which can be written as

$$F_i^{(a)} = a_{ij} W_j + \gamma c_{ij}\dot{W}_j, \quad j = 1,2,\ldots,N, \;\; i = 1,2,\ldots,N. \tag{19}$$

The first term on the right-hand side of Eq. (19) corresponds to the third term in the constitutive equation (9a), containing the first derivative with respect to ξ, and give rise to coupling between different flutter vibrating modes. If the series expansion (10) is taken into account, it is true that [13]

$$a_{ij} = \sigma_d \int_0^1 f_i(\xi)\frac{\partial f_i(\xi)}{\partial \xi}\,\mathrm{d}\xi. \tag{20}$$

The second term is the aerodynamic damping, and corresponds to the last term in Eq. (9a). Thus if the expressions of the linear and non-linear structural forces potential, (11) and (16), respectively, together with the kinetic energy expression (12) and the generalized aerodynamic forces $F_i^{(a)}$ expression (19), are substituted into Eq. (18), one obtains

$$\left[k_{ij}^* + \frac{\alpha}{2}\varphi_{ij}\varphi_{kl} W_k W_l\right] W_j + m_{ij}\ddot{W}_j + \gamma c_{ij}\dot{W}_j = 0, \quad j = 1,2,\ldots,N, \;\; i = 1,2,\ldots,N, \tag{21}$$

where the elements

$$k_{ij}^{*} = k_{ij} + a_{ij} \tag{22}$$

take into account both the linear structural and aerodynamic forces [13]. The matrix [**B**] of the elements

$$b_{ij} = k_{ij}^{*} + \frac{\alpha}{2}(\varphi_{kl} W_k W_l)\varphi_{ij} \tag{23}$$

and the mass matrix [**M**] are introduced. The column vectors [**W**] and [**Z**] of the series expansions (10) coefficients W_i and their first derivatives $\dot{W}_i$ versus time τ, respectively, are also introduced. If Eqs. (13) and (14) are taken into account, the system of equations in time (21) is equivalent to the system written in normal matrix form:

$$\begin{aligned} [\mathbf{Z}] &= [\dot{\mathbf{W}}], \\ [\dot{\mathbf{Z}}] &= -[\mathbf{M}]^{-1}[\mathbf{B}][\mathbf{W}] - \frac{\gamma}{\lambda}[\mathbf{Z}]. \end{aligned} \tag{24}$$

There exist good algorithms for the integration in time, which can give accurate results.

In the simply supported beam case, it is easy to apply the Galerkin method for solving the differential equations in ξ, and then to start the integration process in time, as in Dowell's model [1]. This is reported in Appendix B.

Also the FEM can be utilized to find a solution of the differential problem in the axial coordinate ξ, and reduce the dependence only on time, as shown in Appendix C.

3. Applications and results

The computational algorithms have been applied in two cases of a beam, with both simply supported and clamped ends (as shown in Fig. 1). The ratio between the beam length L and its thickness h is supposed equal to 100, and consequently the non-dimensional parameter α is equal to 120 000. For the number N of the describing functions in Eq. (10), it has been chosen $N = 8$.

Different from the linear case, for a pre-established dynamic pressure, there are infinite solutions for a vibrating mode, which can vary in a frequency range with continuity, and there is correspondence between the amplitude of a vibrating mode with its frequency, that is each frequency has its amplitude.

First the case of a simply supported beam is considered. In Fig. 2 the behaviour of the amplitude a_m, multiplied by 100, of the first two vibrating modes without damping versus the non-dimensional frequency parameter ω_d, which is connected with the true frequency via the following relation

$$\omega_d^2 = \omega^2 \frac{\mu L^4}{EI} \tag{25}$$

is shown with a continuous line for $\sigma_d = 800$. Both modal shapes start from the frequency ω_{min}, where they coalesce, and continue to diverge versus ω_d. Such behaviour has been obtained by the data points in Table 1, which in Fig. 2 appear as dots.

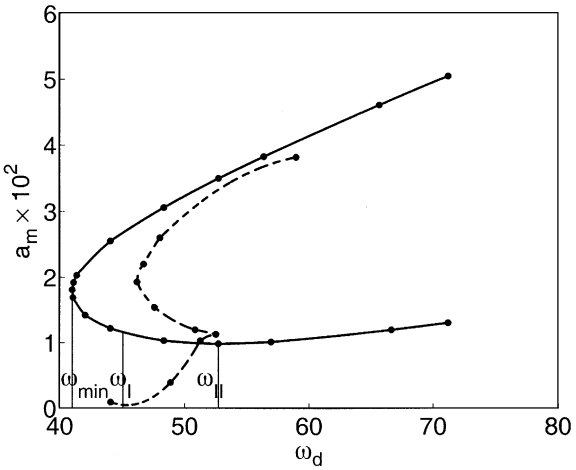

Fig. 2. Behaviour of the modal shape amplitude $a_m \times 10^2$ versus the frequency parameter ω_d of the simply supported undamped beam, and the evolution of the damped beam vibration state towards the limit cycle.

Table 1
Values of the modal amplitude $a_m \times 10^2$ versus the non-dimensional frequency parameter ω_d in the simply supported beam case

ω_d	$a_m \times 10^2$
71.19	5.05
65.66	4.61
56.39	3.83
52.75	3.50
48.32	3.06
44.04	2.55
41.35	2.03
41.11	1.92
41.00	1.81
41.06	1.69
42.04	1.42
44.04	1.22
48.32	1.03
52.75	0.99
56.98	1.01
66.63	1.20
71.19	1.31

It is interesting to remark that in the lower amplitude mode the first derivative $\partial W/\partial\xi$ at $\xi = 0$ of the bending displacement, chosen as a variable parameter characterizing the modal shape, at a frequency a little smaller than ω_I is positive and very little, becomes zero for $\omega_I = 45.06$ and then becomes negative for $\omega_d > \omega_I$, but its modulus grows with the frequency. This can be deduced from Figs. 3 and 4, where both modal shapes for $\omega_d = 44.04$ and 48.32, a little lower and higher than ω_I, respectively, are shown. Consequently, from ω_I and over there is a second half-wave

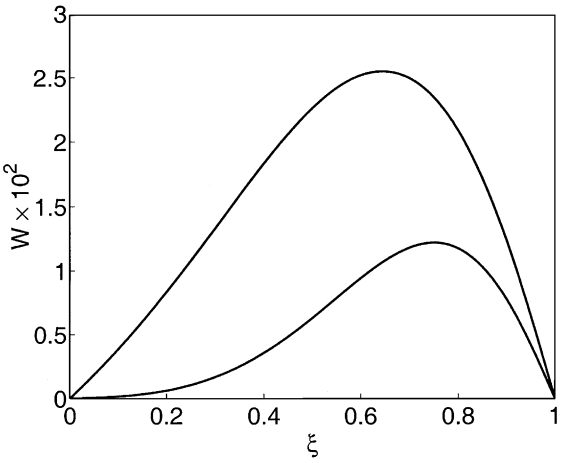

Fig. 3. Modal shapes of the simply supported beam at a frequency a little lower than ω_I.

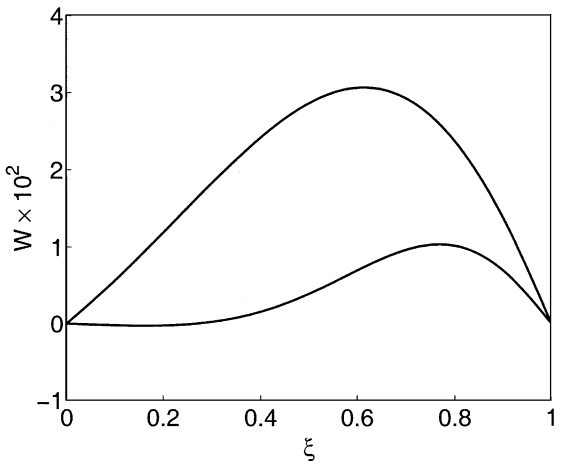

Fig. 4. Modal shapes of the simply supported beam at a frequency a little higher than ω_I.

negative. This above-mentioned frequency is particularly important because it separates two frequency ranges, where there are modal shapes with only one half-wave and two half-waves, respectively.

As the frequency increases further, the lower modal shape amplitude diminishes till a minimum in $\omega_{II} = 52.75$, then it starts to increase, while the amplitude of the other larger modal shape with only one half-wave continues to grow indefinitely. In the frequency range $\omega_I \leqslant \omega_d \leqslant \omega_{II}$ it must be also pointed out that in this lower mode the negative second half-wave amplitude increases, while the larger positive half-wave amplitude (which coincides with the whole modal shape amplitude) decreases. It means that from ω_I and over, the second natural vibrating mode presence in the lower mode becomes more and more consistent, besides the first one, while the influence of the other modes is very small.

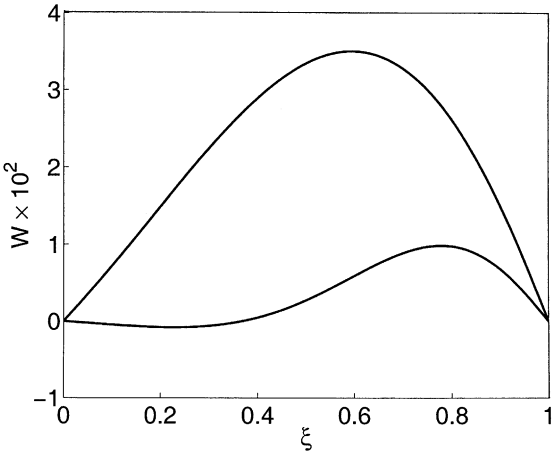

Fig. 5. Modal shapes of the simply supported beam at the frequency ω_{II} without aerodynamic damping.

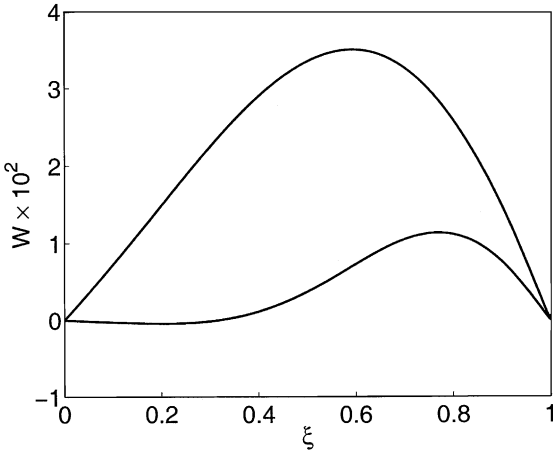

Fig. 6. Modal shapes of the simply supported beam higher amplitude mode at the frequency ω_{II} without aerodynamic damping, and in limit cycle flutter conditions.

The two modal shapes at the frequency ω_{II} without damping, corresponding in Fig. 2 to point U of minimum amplitude and V of the bigger amplitude mode, respectively, are shown in Fig. 5. In Fig. 6 the lower amplitude mode is the flutter limit cycle modal shape, obtained taking into account the aerodynamic damping, corresponding to point T of Fig. 2, while the higher amplitude mode is the same as Fig. 5. From Figs. 5 and 6 it is possible to deduce that the modal shape of the beam flutter limit cycle (point T in Fig. 2) is nearly coincident with the one of the beam without damping for $\omega_d = \omega_{II}$ and with minimum amplitude (point U in the same Fig. 2).

In Fig. 2 also the behaviour of the beam flutter state evolution, obtained by the complete model with aerodynamic damping, towards point T of the limit flutter conditions, very close to point U of the minimum amplitude undamped solution, is sketched with two dashed lines for two cases with different starting conditions. The dots in the upper and lower branches of the system evolution, correspond to different dynamic states of the beam at various values of the

Table 2
Values of the modal amplitude versus the non-dimensional frequency parameter ω_d at various time instants in the simply supported beam flutter case with aerodynamic damping

τ	$a_m \times 10^2$	ω_d
Upper		
0.0	58.97	3.82
0.18	48.0	2.6
0.21	46.7	2.2
0.36	46.18	1.93
0.50	47.58	1.54
0.88	52.12	1.15
1.0	52.55	1.13
Lower		
0.0	44.07	0.10
0.14	48.87	0.39
0.51	52.55	1.13

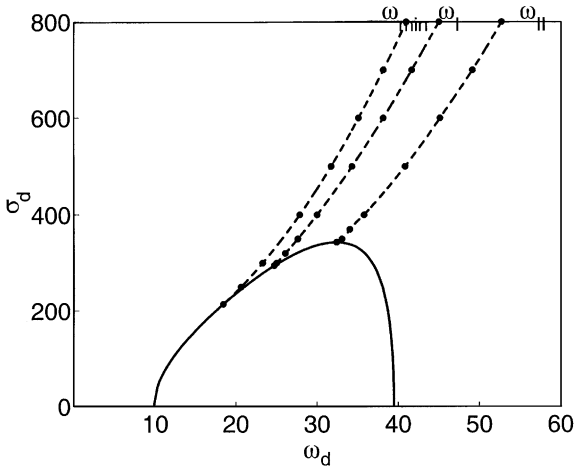

Fig. 7. Behaviours of the three frequencies ω_{min}, ω_I and ω_{II} versus σ_d, and the behaviour of σ_d versus ω_d of the linearized model of the simply supported beam.

non-dimensional time τ. The corresponding data points have been reported in Table 2. The aerodynamic damping force is supposed to be equal to $0.005\sigma_d \partial W/\partial\tau$.

The behaviours of the three frequencies ω_{min}, ω_I and ω_{II} versus the dynamic pressure non-dimensional parameter σ_d, are shown in Fig. 7 with three dashed lines, together with the behaviour $\sigma_d - \omega_d$ of the linear case with a continuous line. It is quite evident that the behaviours of ω_{min} and ω_I converge at two points on the left branch of the idealized and linearized model curve without damping, whereas ω_{II} converges towards the critical conditions point of the same linear beam model. This fact can be explained considering that the minimum mode amplitude at $\omega = \omega_{II}$ diminishes with σ_d, and vanishes when this parameter reaches the linear beam flutter

Table 3
Values of the frequencies ω_{min}, ω_I and ω_{II} versus the non-dimensional dynamic pressure parameter σ_d in the simply supported beam case

σ_d	ω_{min}	ω_I	ω_{II}
800	41.00	45.06	52.75
700	38.17	41.68	49.19
600	35.12	38.16	45.20
500	31.74	34.32	40.86
400	27.90	30.03	35.79
370			34.05
350		27.66	33.08
343.356			32.433
320		26.13	
300	23.34	25.06	
294.6		24.76	
250	20.65		
214	18.46		

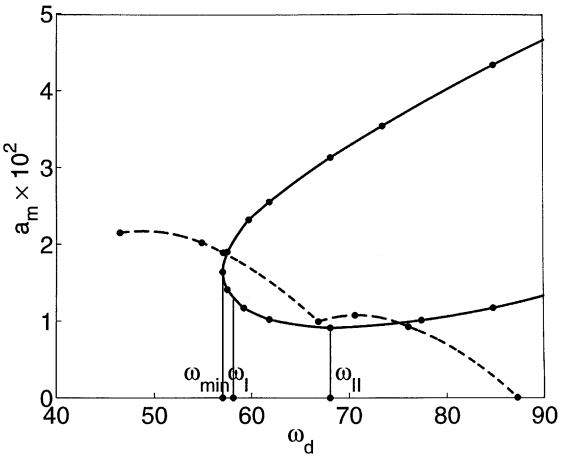

Fig. 8. Behaviour of the modal shape amplitude $a_m \times 10^2$ versus the frequency parameter ω_d of the clamped undamped beam, and the evolution of the damped beam vibration state towards the limit cycle.

critical value, and the non-linear force contribution becomes more and more negligible with the diminishing modal amplitude.

The data points by which the three behaviours of the simply supported beam have been built, corresponding to the dots of Fig. 7, are reported in Table 3.

Now the results obtained for the beam clamped at both ends will be analyzed. In Fig. 8 the behavior of the amplitude a_m of the first two vibrating modes, multiplied by 100, versus frequency without damping and in steady conditions, for $\sigma_d = 1000$, is shown with a continuous line, where the dots are the data points of Table 4. In this case of a beam clamped at both ends, the first derivative $(\partial W/\partial \xi)$ at $\xi = 0$, cannot be a significative parameter because it vanishes at the ends,

Table 4
Values of the modal amplitude $a_m \times 10^2$ versus the non-dimensional frequency parameter ω_d in the clamped beam case

ω_d	$a_m \times 10^2$
84.70	4.33
73.36	3.54
68.03	3.13
61.79	2.55
59.70	2.32
57.52	1.90
57.082	1.72
57.04	1.64
57.21	1.50
57.52	1.41
59.20	1.17
61.79	1.022
68.03	0.911
77.39	1.01
84.70	1.17

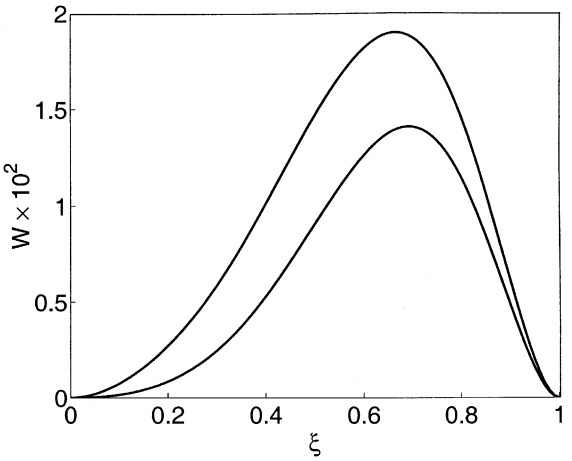

Fig. 9. Modal shapes of the clamped beam at a frequency a little lower than ω_I.

and the second derivative $\partial^2 W/\partial\xi^2$ at $\xi = 0$ is chosen as a parameter characterizing the modal shape of the clamped vibrating beam.

It must be pointed out that this parameter of the curvature at $\xi = 0$, for the lower amplitude mode and at a frequency a little smaller than ω_I is positive and very small, vanishes for $\omega_I = 58.15$ and then becomes negative for $\omega_d > \omega_I$, but its modulus grows with the frequency. This can be deduced from Figs. 9 and 10, where both modal shapes for the two frequencies $\omega_d = 57.52$ and 61.79, a little lower and higher than ω_I, respectively, are shown.

As the frequency increases further, the lower mode amplitude diminishes till a minimum at $\omega_{II} = 68.03$, then it starts to increase, while the amplitude of the other larger modal shape with only one half-wave continues to grow indefinitely. The whole behaviour is very similar to the

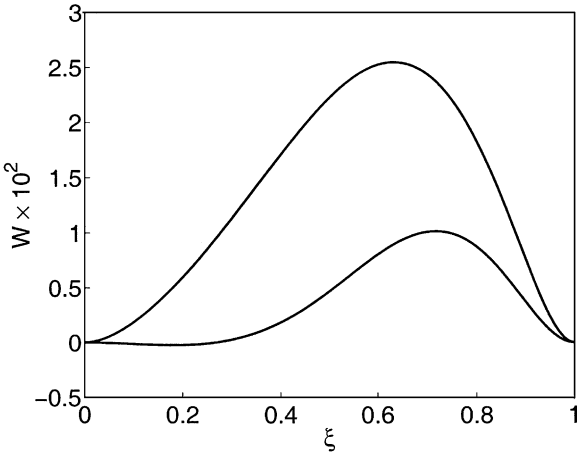

Fig. 10. Modal shapes of the clamped beam at a frequency a little higher than ω_I.

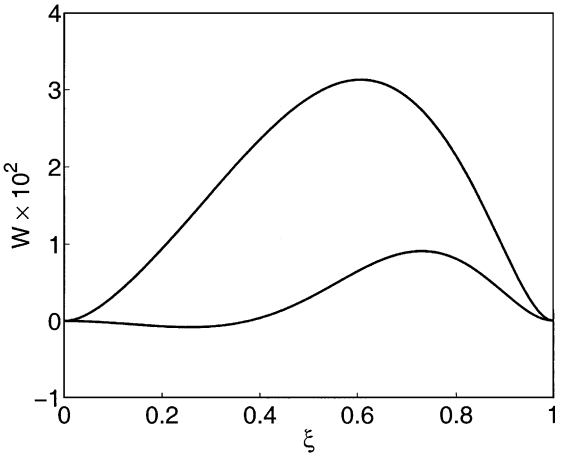

Fig. 11. Modal shapes of the clamped beam at the frequency ω_{II} without aerodynamic damping.

previous one of the simply supported beam, and the same characteristics of the flutter vibration versus the frequency can be seen.

The modal shapes at the frequency ω_{II} are shown in Fig. 11 in the undamped beam case, corresponding to points U and V in Fig. 8, respectively, whereas in Fig. 12 the lower amplitude mode corresponds to the limit flutter cycle of the damped beam (point T in Fig. 8), and the higher amplitude mode is the same as in Fig. 11. From Figs. 11 and 12 it is possible to emphasize that also in the clamped beam case the modal shape of the limit cycle flutter solution is nearly coincident with the corresponding one of a beam without damping for $\omega_d = \omega_{II}$ and with minimum amplitude (point U of the same Fig. 8).

In Fig. 8 also the behaviour of the beam flutter state evolution, obtained by the complete model with aerodynamic damping, towards point T of the limit cycle flutter solution, is sketched with two dashed lines for two cases with different starting conditions, if the aerodynamic damping force is supposed to be equal to $0.01\sigma_d \partial W/\partial\tau$. The dots in the left and right branch of the system

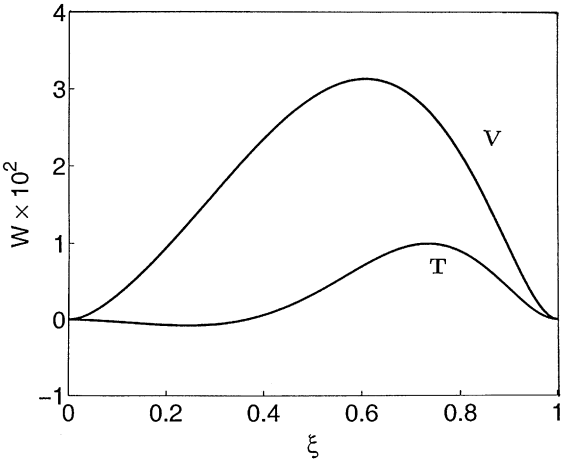

Fig. 12. Modal shapes of the clamped beam higher amplitude mode at the frequency ω_{II} without aerodynamic damping, and in limit cycle flutter conditions.

Table 5
Values of the modal amplitude versus the non-dimensional frequency parameter ω_d at various time instants in the clamped beam flutter case with aerodynamic damping

τ	$a_m \times 10^2$	ω_d
Left		
0.0	46.51	2.15
0.359	54.9	2.02
0.725	57.09	1.89
1.815	66.81	0.993
Right		
0.0	87.22	0.0003
0.378	76.03	0.93
2.364	70.57	1.076
8.034	66.81	0.993

evolution, correspond to different dynamic states of the beam at various values of the non-dimensional time τ, as reported in Table 5.

It is possible to notice that also in the clamped beam case the fluttering state evolution with aerodynamic damping converge towards a point T, corresponding to the limit flutter conditions, which is very close to point U representative of the vibrating beam solution without damping and with minimum amplitude.

The behaviours of the three frequencies ω_{min}, ω_I and ω_{II} versus the dynamic pressure non-dimensional parameter σ_d, are shown in Fig. 13 with three dashed lines. It is evident enough that the behaviour of ω_{min} and ω_I converge at a point on the left branch of the idealized and linearized flutter model curve, shown in the same figure with a continuous line, whereas ω_{II} converges towards the critical conditions point of the same linear beam model, like in the simply supported beam case.

The data points, which appear as dots in Fig. 13, are reported in Table 6.

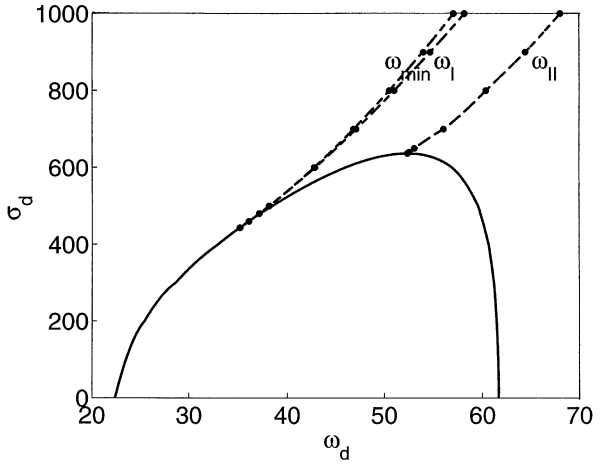

Fig. 13. Behaviours of the three frequencies ω_{min}, ω_I and ω_{II} versus σ_d, and the behaviour of σ_d versus ω_d of the linearized model of the clamped beam.

Table 6
Values of the frequencies ω_{min}, ω_I and ω_{II} versus the non-dimensional dynamic pressure parameter σ_d in the clamped beam case

σ_d	ω_{min}	ω_I	ω_{II}
1000	57.04	58.15	68.03
900	53.89	54.67	64.38
800	50.50	51.01	60.36
700	46.83	47.11	56.02
650			53.07
640			52.54
636.569			52.358
600	42.76	42.86	
500	38.16	38.17	
480	37.16	37.16	
460	36.12	36.12	
443.3	35.22	35.22	

4. Conclusions

This numerical procedure, which utilizes the Rayleigh–Ritz method, is very efficient to determine approximately all the possible solutions without damping in the frequency range from a minimum ω_{min} and over, after an integration process in time. Also the Galerkin method in the first case, with $N = 20$ in Eq. (B.1), as in Dowell's numerical model [1], and the FEM with $N_E = 12$, in both cases have been employed in the same solving approach, and the same results have been obtained, but with a lower convergence rate.

The starting conditions ($\tau = 0$) of the resulting mode components necessary to find all the stationary solutions of the undamped beam are not known a priori, but they can be determined by an approximate method where the axial strain is supposed constant versus the time, after an appropriate correction is performed.

The final purpose of the work focuses on the possibility of foreseeing with a good approximation the main characteristics of the beam dynamic solution in limit cycle flutter conditions with aerodynamic damping, and explains the reason for that. In fact by the model utilized it has been possible to perform a complete analysis of the all the solutions of the fluttering beam without damping to individuate the area where there is possibility of finding the flutter limit cycle presence, which lies in the neighbourhood of the one with minimum amplitude.

This can be deduced by intuitive considerations for the following reasons. Since the aerodynamic damping is small, the limit flutter cycle solution lies in the neighbourhood of some undamped beam vibration solution, and this must be the one with minimum amplitude. In fact starting from higher amplitude values, although there exist permanent solutions without damping, the presence of these passive aerodynamic forces diminishes in time the modal shape amplitude and the point representative of the vibration state moves towards point T, which is very close to the undamped beam minimum amplitude point U, as in Figs. 2 and 8. On the other hand, starting from lower amplitude values, the coupling aerodynamic forces are large enough to increase the vibrating mode amplitude, and for this reason there is no possibility of permanent vibration solutions with and without aerodynamic damping, and likewise the representative point moves towards point T in the same figures. Consequently, it is possible to find the limit flutter cycle only around this minimum amplitude undamped beam solution. It has been possible to verify such limit cycle presence in this area by the complete model with damping.

This procedure has been applied to uni-dimensional vibrating structures, but surely the same concluding remarks are valid for bi-dimensional vibrating panels cases.

Appendix A

The expressions of the describing functions of the series expansion (10), when a procedure which arises from the Rayleigh–Ritz method is utilized, must be considered.

For the simply supported beam these describing functions, which satisfy only the geometric boundary conditions, for which they vanish at both ends, are:

$$f_i(\xi) = \xi^i(1-\xi), \quad f_j(\xi) = \xi^j(1-\xi), \quad i,j = 1,2,\ldots,N \tag{A.1}$$

whose first derivatives with respect to ξ can be easily determined, and consequently the integrals φ_{ij} of Eq. (15b), are equal to

$$\varphi_{ij} = \frac{ij}{(i+j-1)} - \frac{i(j+1)+(i+1)j}{(i+j)} + \frac{(i+1)(j+1)}{(i+j+1)}. \tag{A.2}$$

In the case of the clamped beam these describing functions, which for the geometric boundary conditions vanish with their first axial derivatives at both ends, can be written as

$$f_i(\xi) = \xi^{i+1}(1-\xi)^2, \quad f_j(\xi) = \xi^{j+1}(1-\xi)^2, \quad i,j = 1,2,\ldots,N \tag{A.3}$$

and also as

$$f_i = s_k \xi^{i+1+k}, \quad f_j = s_l \xi^{j+1+l}, \quad k, l, = 0, 1, 2, \tag{A.4a}$$

$$s_0 = 1, \quad s_1 = -2, \quad s_2 = 1. \tag{A.4b}$$

Thence, after their first derivatives have been evaluated, the same integrals can be obtained:

$$\varphi_{ij} = (i + 1 + k)(j + 1 + l) \frac{1}{(i + j + k + l + 1)} s_k s_l, \quad k, l = 0, 1, 2. \tag{A.5}$$

Appendix B

As in the Ritz procedure the linear terms of the Galerkin method in the case of a simply supported beam have been previously evaluated [13], and so only the non-linear ones are considered.

A trigonometric series expansion for the bending displacement W is chosen, as follows:

$$W(\xi, \tau) = W_i(\tau) \sin(i\pi\xi), \quad i = 1, 2, \ldots, N, \tag{B.1}$$

because these describing functions $\sin(i\pi\xi)$ satisfy both the geometric and the natural boundary conditions, for which these along with their second axial derivatives vanish at both ends.

This series expansion can be substituted into Eq. (9a), then by pre-multiplying by the generic describing function and integrating one obtains the dynamic constitutive equation:

$$[\textit{linear terms}]_i + \alpha(i\pi)^2 \varepsilon_x \frac{W_i(\tau)}{2} = 0, \quad i = 1, 2, \ldots, N \tag{B.2}$$

similar to Eq. (21), where from expression (15a) of ε_x it is true that

$$\varepsilon_x = \frac{\pi^2}{4} k^2 W_k^2, \quad k = 1, 2, \ldots, N. \tag{B.3}$$

An equations system in normal matrix form, as in Eq. (24), is obtained, where both the mass matrix [**M**] and the stiffness matrix [**K**] are diagonal.

Appendix C

Also the FEM can be utilized in both cases. As for the Ritz and Galerkin procedures the linear terms in the dynamic constitutive equation have been previously determined [13], and consequently only the non-linear ones will be taken into account.

The beam is divided into N_E elements and the i_eth element lies between the sections S_{i_e-1} and S_{i_e}, with non-dimensional axial co-ordinates ξ_{i_e-1} and ξ_{i_e}, respectively.

It is useful to introduce a non-dimensional normalized axial co-ordinate for each i_eth element, as follows:

$$\xi_n = (\xi - \xi_{i_e-1}) N_E, \quad \xi_{i_e-1} \leqslant \xi \leqslant \xi_{i_e}, \quad 0 \leqslant \xi_n \leqslant 1. \tag{C.1}$$

The non-dimensional flexural displacement $W(\xi)$ expression in the i_eth element versus this normalized axial co-ordinate is [13]

$$W(\xi_n) = C_{i_p}^{(i_e)} \phi_{i_p}^{(i_e)}(\xi_n), \quad i_p = 1,2,3,4, \tag{C.2}$$

where:

$$\begin{aligned} C_1^{(i_e)} &= W_{i_e-1}, \quad \phi_1^{(i_e)} = 1 - 3\xi_n^2 + 2\xi_n^3, \\ C_2^{(i_e)} &= \theta_{i_e-1}, \quad \phi_2^{(i_e)} = \xi_n - 2\xi_n^2 + \xi_n^3, \\ C_3^{(i_e)} &= W_{i_e}, \quad \phi_3^{(i_e)} = 3\xi_n^2 - 2\xi_n^3, \\ C_4^{(i_e)} &= \theta_{i_e}, \quad \phi_4^{(i_e)} = \xi_n^3 - \xi_n^2 \end{aligned} \tag{C.3}$$

and W_{i_e} is the non-dimensional flexural displacement on the section S_{i_e}, θ_{i_e} is a rotation parameter, equal to the true rotation on the same section divided by N_E.

The expression of W throughout the beam length can be written in a series expansion form, as in Eq. (10):

$$W(\xi) = W_i f_i(\xi), \quad i = 1,2,\ldots,N, \tag{C.4}$$

where the generic coefficient W_i in the i_eth element is equal to one of the four coefficients $C_{i_p}^{(i_e)}$, and the generic describing function $f_i(\xi)$ is equal to an introduced one $\phi_{i_p}^{(i_e)}$ in Eq. (C.2). These describing functions at the beam ends, as in the Ritz procedure, satisfy only the geometric boundary conditions.

The indices i and i_p for the simply supported beam in the i_eth element are connected via the following relation:

$$i = 1 + 2(i_e - 2) + i_p, \quad i_p = 1,2,3,4 \tag{C.5}$$

if $1 < i_e < N_E$, while for the clamped beam one has for the same values of i_e:

$$i = 2(i_e - 2) + i_p, \quad i_p = 1,2,3,4. \tag{C.6}$$

For $i_e = 1$ and the simply supported beam, expression (C.5) is valid, but for $i_p = 2,3,4$, while for the clamped beam expression (C.6) is valid, but with $i_p = 3,4$.

For $i_e = N_E$ and the simply supported beam, Eq. (C.5) must be changed into

$$i = 1 + 2(i_e - 2) + i_p - \frac{i_p}{3}, \quad i_p = 1,2,4, \tag{C.7}$$

that is i_p cannot be equal to 3, while for the clamped beam equation (C.6) is valid, but with $i_p = 1,2$.

For the above-mentioned reasons the whole number N of Lagrangian degrees of freedom is connected with the number N_E of elements of FEM model via the following expression:

$$N = 2N_E \tag{C.8a}$$

for the simply supported beam and:

$$N = 2(N_E - 1) \tag{C.8b}$$

for the clamped beam.

The integrals in Eq. (15b) can be thus obtained:

$$\varphi_{ij} = N_E \int_0^1 \frac{\partial \phi_{i_p}^{(i_e)}}{\partial \xi_n} \frac{\partial \phi_{j_p}^{(j_e)}}{\partial \xi_n} \mathrm{d}\xi_n, \quad i = i(i_e, i_p), \quad j = j(j_e, j_p), \tag{C.9}$$

taking into account that $\mathrm{d}\xi = \mathrm{d}\xi_n / N_E$. From integral (C.9) it is possible to evaluate the strain ε_x. Also in the FEM model the stiffness and mass matrices have been already determined [13], which allows one to arrive at the constitutive equation (21) and a system of equations written in normal matrix form, as in Eq. (24).

Appendix D. Nomenclature

A_s	beam cross-sectional area equal to $b_w h$
b_w	beam width
c_d	dimensional aerodynamic damping coefficient
c_{ij}	coupling elements between the describing functions of the bending displacements
$C_{i_p}^{(i_e)}$	generic coefficient of the non-dimensional flexural displacement behaviour series expansion in the i_eth element of FEM model
E	elasticity modulus
$F_i^{(a)}$	aerodynamic generalized forces
$f_i(\xi)$	trial describing functions of the non-dimensional flexural displacement behaviour throughout the beam length
h	thickness of the beam rectangular cross-section
I	flexural moment of inertia of the beam equal to $b_w h^3/12$
h	beam thickness
k_{ij}	stiffness matrix elements
k_{ij}^*	linear structural and aerodynamic forces resultant matrix elements
L	beam length
M_{ach}	Mach number
m_{ij}	mass matrix elements
N	whole number of the degrees of freedom
N_x	resulting axial strength
q	dynamic pressure equal to $\frac{1}{2}\rho u_\infty^2$
t	state evolution time
T_o	reference time
U_∞	speed of flow
u	axial displacement
w	flexural displacement
W_i	generic coefficient of the non-dimensional flexural displacement behaviour series expansion
W	non-dimensional flexural displacement

W_{i_e} non-dimensional flexural displacement in a generic i_eth section of the beam FEM model
x beam axial axis

Greek symbols
α beam axial rigidity non-dimensional parameter
β non-dimensional Mach number parameter equal to $(M_{ach}^2 - 1)^{1/2}$
γ non-dimensional aerodynamic damping coefficient
ε_x beam axial strain
θ_{i_e} rotation parameters in a generic i_eth section of the beam FEM model
λ non-dimensional mass distribution parameter
μ mass per unit length of the beam
ξ non-dimensional axial co-ordinate of the beam
ξ_n normalized non-dimensional axial co-ordinate of a beam element in FEM model
ρ air density
σ dimensional dynamic pressure parameter
σ_d non-dimensional dynamic pressure parameter
τ non-dimensional time
ϕ_{i_p} describing function in the i_eth element of the beam FEM model
φ_{ij} integral of the product between the first derivatives of the describing functions $f_i(\xi)$ and $f_j(\xi)$
ω angular frequency
ω_d dimensionless frequency parameter

Special symbols
∂ partial differentiation
[B] structural and aerodynamic forces matrix
[K] stiffness matrix
[M] mass matrix
$\mathscr{T}$ kinetic energy expression
$\mathscr{U}_l$ potential of the linear structural forces
$\mathscr{U}_{nl}$ potential of the non-linear structural forces

Subscripts
i, j subscripts referring to functions and coefficients of the flexural displacement behaviour series expansion
i_e subscript referring to the $(i_e + 1)$th section of FEM model
i_p, j_p subscripts in the series expansion of the flexural displacement in the generic element of the beam FEM model

Superscripts
$(i_e), (j_e)$ superscripts referring to the i_eth, j_eth element of FEM model

References

[1] E.H. Dowell, Nonlinear oscillations of a fluttering plate, American Institute of Aeronautics and Astronautics Journal 4 (1966) 1267–1275.
[2] E.H. Dowell, Nonlinear oscillations of a fluttering plate—II, American Institute of Aeronautics and Astronautics Journal 5 (1967) 1856–1862.
[3] L.V. Kantorowich, V.I. Krylov, Approximate Methods of Higher Analysis, Interscience, Inc., New York, 1964, pp. 258–303.
[4] S.G. Mikhlin, Variational Methods in Mathematical Physics, Pergamon Press, Oxford, 1964, pp. 74–125, 448–490.
[5] C.C. Kuo, L. Morino, J. Dugundji, Perturbation and harmonic methods for nonlinear panel flutter, American Institute of Aeronautics and Astronautics Journal 10 (1972) 140–145.
[6] L.L. Smith, L. Morino, Stability analysis of nonlinear differential autonomous systems with applications to flutter, American Institute of Aeronautics and Astronautics Journal 14 (1976) 333–341.
[7] W. Weaver Jr., P.R. Johnston, Finite Elements for Structural Analysis, Prentice-Hall, Englewood Cliffs, NJ, 1984, pp. 1–102.
[8] J.N. Reddy, C.S. Krishnamoorthy, K.N. Seetharamu, Finite Element Analysis for Engineering Design, Springer, Berlin, 1988, pp. 41–89, 274–309.
[9] J. Qin, C.E. Gray Jr., C. Mei, Vector unsymmetric eigenequation solver for non-linear flutter analysis on high performance computers, Journal of Aircraft 30 (1993) 744–750.
[10] R.L. Bisplinghoff, Principles of Aeroelasticity, Wiley, New York, 1962, pp. 108–114.
[11] E.H. Dowell, H.C. Curtis Jr., R.H. Scanlan, F. Sisto, A Modern Course in Aeroelasticity, Sijthoff and Noordhoff, Alphen aan den Rijn, The Netherlands, 1980, pp. 81–91.
[12] S. Tizzi, Study of a numerical procedure for the vibrating structure analysis, Strojnicky Casopis (Slovak Republic) 45 (Pt I) (1994) 189–197, (Pt II) 285–298.
[13] S. Tizzi, A numerical procedure for the analysis of a vibrating panel in critical flutter condition, Computers and Structures 50 (1994) 299–316.
[14] S. Tizzi, Application of a numerical procedure for the dynamic analysis of plane aeronautical structure, Journal of Sound and Vibration 193 (1996) 957–983.
[15] J.N. Reddy, Applied Functional Analysis and Variational Methods in Engineering, McGraw-Hill, New York, 1986, pp. 258–285.
[16] L.A. Pars, A Treatise on Analytical Dynamics, Heinemann Educational Books, Ltd., London, 1968, pp. 28–89.
[17] P. Santini, Introduzione alla Teoria delle Strutture, Tamburini Editore, Milano, 1973, pp. 176–181.